UDK/*UDC*: 532.5:627(047.31)(575.1)
Izvirni znanstveni članek – *Original scientific paper*
DOI: 10.15292/acta.hydro.2025.01
Prejeto/*Received:* 29.10.2024
Sprejeto/*Accepted:* 26.03.2025
Objavljeno na spletu/*Published online:* 05.05.2025

NUMERICAL SIMULATION OF THE FLOW RECTIFICATION MEASURES IN THE FOREBAY OF THE PUMPING STATION

NUMERIČNE SIMULACIJE UKREPOV ZA URAVNAVANJE PRETOKA V VTOČNEM BAZENU ČRPALIŠČA

Aybek Arifjanov[1], Alimardon Sattorov[2], Murodil Madaliyev[2], Zokhidjon Abdulkhaev[2,*], Mamadali Madrakhimov[2]

[1]Tashkent Institute of Irrigation and Agricultural Mechanization Engineers National Research University, Uzbekistan

[2] Fergana State Technical University, Uzbekistan

Abstract

The kinematics of flow movement in the forebays of pumping stations significantly influence the efficiency of pump operation. This study addresses the issue of sediment accumulation caused by improper flow velocity distribution in the intake structures of pumping stations. Research was conducted at the water intake structure of Uzbekistan's Dehqonobod pumping station, located in Quva district, Fergana region. The study involved analyzing hydrodynamic processes within the intake structure based on the principles of fluid motion, combining experimental approaches with simulations using the COMSOL Multiphysics software suite to develop a 3D structural model of the prototype intake structure. Additionally, numerical simulations were performed using the Newton-Raphson scheme and the realizable k-ε turbulence model for comparative analysis and evaluation. To ensure proper flow velocity distribution, six vertical columns were arranged in a triangular pattern relative to the flow movement, with a spacing of 1 meter between them. This arrangement was proposed so as to enhance technical and economic efficiency. The results of the study demonstrated that the installation of vertical columns increased the flow velocity near the right and left walls of the forebay, achieving a variation in velocity distribution of up to 20%. Specific recommendations were developed to optimize the hydrodynamic conditions and improve the pumping station's operational efficiency.

Keywords: flow pattern, flow velocity, flow regulating columns, k-ε model, finite volume model, rectification scheme, Navier–Stokes equations.

Izvleček

Gibanje toka v vtočnih bazenih črpališč pomembno vpliva na učinkovitost delovanja črpalk. Študija obravnava vprašanje kopičenja plavin, ki ga povzroča neustrezna porazdelitev pretočnih hitrosti v zajemnih objektih

[*] Stik / *Correspondence*: zokhidjon@fstu.uz

črpališč. Raziskave so bile izvedene na vtoku v črpališče Dehqonobod v okrožju Quva v regiji Fergana, Uzbekistan. Študija je vključevala analizo hidrodinamičnih procesov znotraj zajemnega objekta na podlagi principov gibanja tekočin, pri čemer smo eksperimentalne pristope kombinirali s simulacijami z uporabo programske opreme COMSOL Multiphysics za razvoj 3D strukturnega modela prototipnega zajemnega objekta. Poleg tega so bile za primerjalno analizo in oceno izvedene numerične simulacije z uporabo Newton-Raphsonove sheme in realizacijski k-ε turbulentni model. Da bi zagotovili pravilno porazdelitev pretočnih hitrosti, je bilo šest navpičnih stebrov razporejenih v trikotnem vzorcu glede na gibanje toka, razdalja med njimi je bila 1 meter. Ta ureditev je bila predlagana za povečanje tehnične in ekonomske učinkovitosti. Rezultati študije so pokazali, da je namestitev navpičnih stebrov povečala hitrost toka v bližini desne in leve stene vtočnega bazena in dosegla do 20-odstotno spremembo v porazdelitvi hitrosti. Pripravljena so bila posebna priporočila za optimizacijo hidrodinamičnih pogojev in izboljšanje obratovalne učinkovitosti črpališča.

Ključne besede: vzorec pretoka, pretočna hitrost, stebri za uravnavanje pretoka, k-ε model, model volumna tekočine, rektifikacijska shema, Navier-Stokesove enačbe.

1. Introduction

The forebay of a pumping station is a crucial transitional zone between the water source and the pump intake. This zone plays a significant role in efficiently managing water flow and ensuring the proper velocity distribution, both of which are essential for maintaining optimal operating conditions for the pumping equipment (Arifjanov et al., 2024; Luo et al., 2024). The stability and efficiency of the flow are vital for enhancing the pumping system's overall operational efficiency (Arifjanov et al., 2023; Qiao et al., 2024). Furthermore, the hydraulic conditions in the pump forebay are critical factors that determine the pump's intake capacity and energy consumption (Yang et al., 2021). However, external and internal factors may lead to sedimentation, improper velocity distribution, and various hydraulic phenomena in the forebay, resulting in a decrease in the efficiency of water intake structures (Nasr et al., 2021). To address these issues, stabilizing the velocity distribution within the flow is essential for optimizing the kinematic characteristics in the forebay. This stability makes pumping stations more efficient and more reliable, ultimately improving their operational performance (Zhang et al., 2022). Implementing effective flow management strategies can help mitigate adverse hydraulic phenomena and ensure the optimal performance of water intake structures (Mi et al., 2012). Using computational fluid dynamics (CFD) systems to stabilize flow velocity distribution and analyze flow patterns in forebays addresses several ongoing challenges (Xu et al., 2015). CFD methodologies provide valuable insights into complex flow conditions, helping identify and implement effective solutions (Song et al., 2018). For example, research by Luo et al. (2024) has focused on improving flow structure in pumping station forebays by testing combinations of columns and bottom barriers (Ying et al., 2020). This study employs the Volume of Fluid (VOF) method to simulate flow patterns in pump station forebays, identifying adverse flow phenomena such as vortices and backflows. To address these issues, a combined rectification scheme was developed to reduce sediment deposition, optimize water intake conditions, enhance pump efficiency, and ensure the equipment's stable operation. Research by Shi et al. (2024) employed the RNG k-e turbulence model to improve flow structure and reduce eddy motions. Using the PSO-GP model, we determined the ratio between the height and width of the pillars vertically installed in pumping station forebays and the optimal placement scheme for the threshold and pillars at the water intake were determined (Nasr et al., 2021). Zheng et al. (2023) found that the accumulation of water in the front part of the water intake pumping station is mainly due to a decrease in the water level in front of the suction pipes. Research has shown (Song et al., 2018) that employing structures such as baffles, columns, and flow guides can mitigate undesirable hydraulic phenomena, leading to smoother flow and the better performance of pumping systems. Additionally, the use of computational fluid dynamics (CFD) simulations aids in visualizing flow behaviors and optimizing designs for specific site conditions (Zhang et al., 2022). These insights are crucial for the design and optimization of coastal pumping stations, where unique challenges related to sediment transport and flow dynamics often arise (Xu et al., 2015). Existing research findings indicate that the proposed method of flow rectifiers arranged in a chessboard pattern can effectively improve the flow structure in water intake systems. This method introduces an innovative approach, selected as the optimal solution based on extensive scientific studies, ensuring the efficient enhancement of flow characteristics in the forebay. It has been identified as an effective tool for improving flow dynamics in water intake systems, offering significant benefits for operational efficiency.

Drawing on the previously discussed works (Luo et al., 2024; Song et al., 2018; Xu et al., 2015), the proposed method of arranging flow rectifiers in a chessboard pattern has been shown to effectively improve the flow structure in water intake systems. This innovative approach has been selected as an optimal solution through extensive scientific evaluation, ensuring efficient enhancement of flow characteristics in the forebay. It has proven to be an effective tool for improving flow dynamics, offering substantial benefits in terms of operational efficiency.

2. Site investigation

2.1 Overview of the study area

The study area is located in the Quva district of the Fergana region and includes the PK-864+64 Dehqonobod water intake structure. This structure draws water from the Great Fergana Main Canal and supplies it to the irrigation pumping station.

Currently, the pump station is equipped with five pumps of the "Two-way Inlet Pump Unit PD200-500" model. The water intake structure has an entrance width of b = 2 meters, a slope of i = 0.2, and a total length of L = 12 meters**,** with a water delivery capacity of Q = 2.25 m³/s. Additionally, the angle of the forebay conical expansion is 32°**.**

At present, sediment accumulation is clearly observed on both the left and right walls of the water intake structure (Figure 1)**.** This situation adversely affects the normal operation of the pump station and limits the full functionality of the water intake structure.

Figure 1: *Water intake structure sedimentation.*

Slika 1: *Sedimentacija v zajemnem objektu.*

Figure 2: *Flow velocity measurement process in the water intake structure.*

Slika 2: *Meritve pretočnih hitrosti v zajemnem objektu.*

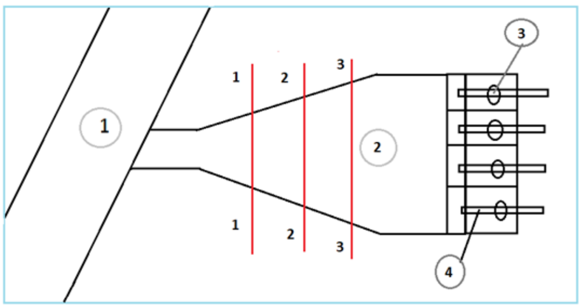

Figure 3: *Structure of the water intake facility.*

Slika 3: *Zajemni objekt.*

The operational period of the Dehqonobod water intake structure extends from March to September. A primary challenge during this period is the uneven distribution of flow velocity within the structure.

Based on the main sedimentation zones, the water intake structure was divided into three cross-sections (Figure 3), where velocity distribution measurements were conducted using the SonTek RS5 Doppler device (Figure 2). The SonTek RS5 Doppler system is an advanced technology widely used for precise velocity measurements in water flow. Utilizing the Doppler Effect, it analyzes particle movement within the flow by measuring the frequency shift of acoustic waves, enabling high-accuracy velocity determination even in challenging conditions. Specifically designed for measuring flow velocity in open channels and water intake structures, this system provides a detailed analysis of flow characteristics, including turbulence and shear stress distribution. Notably, its relative error is limited to just 1%, demonstrating exceptional precision in dynamic environments.

1- Great Fergana main canal, 2- water intake structure, 3-Pump, 4-Suction pipe.

Based on the main sedimentation zones, the water intake structure was divided into three cross-sections (Figure 3), where velocity distribution measurements were conducted using the SonTek-RS5 Doppler device (Figure 2).

3. Computational models and numerical methods

3.1. Model description

The use of vertical columns as an engineering measure to improve the flow regime in the forebay of the pumping station underscores their critical role in enhancing hydraulic efficiency.

The pumping station's water supply channel (1) has a rectangular shape, with the central expansion angle of the forebay (2) clearly defined. To mitigate the formation of large vortex structures typically caused by flow expansion and obstructions, six vertical columns were designed and strategically arranged in a chessboard pattern. This configuration reduces vortex formation in front of the water intake chambers (4) and ensures a more uniform flow velocity distribution.

Figure 4 illustrates the inflow and outflow boundary conditions of the computational domain. The inflow boundary corresponds to the water supply channel (Section 1), while the outflow boundary represents the region at the suction pipes of the pump (Section 5). These boundaries are essential for accurately defining the flow direction and hydrodynamic characteristics of the domain. Such definitions are critical to ensure the reliability and precision of the numerical simulations based on the mathematical model of the flow.

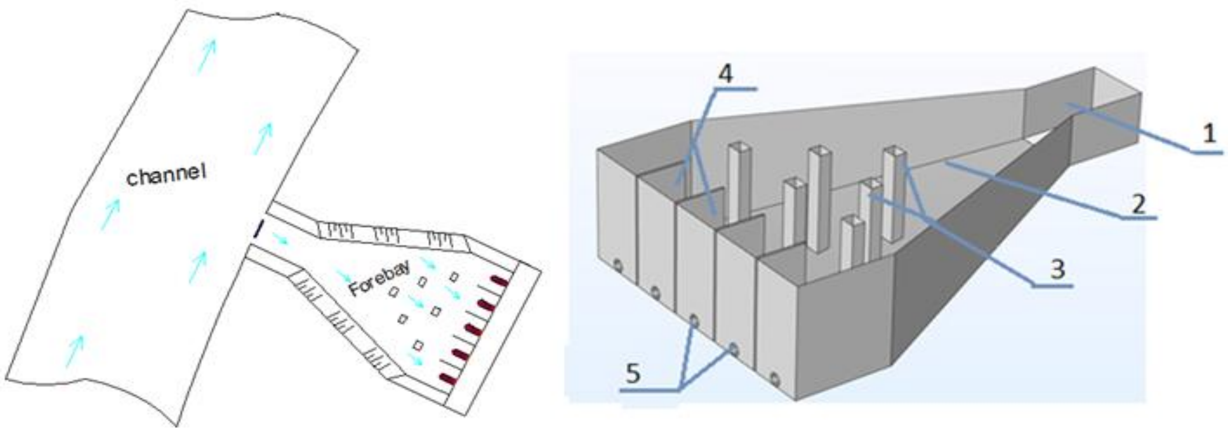

Figure 4: *Calculation model of the pumping station.*

Slika 4: *Računski model črpališča.*

1. Water supply channel, 2. Forebay, 3. Vertical columns of flow adjustment, 4. Water intake chamber, 5. Suction pipes of the pump.

3.2 Governing equations

The fundamental governing equations include the mass conservation equation and the momentum conservation equation. The continuity equation is expressed as follows:

$$\frac{\partial u}{\partial x}+\frac{\partial \vartheta}{\partial y}+\frac{\partial w}{\partial z}=0 \tag{1}$$

The momentum conservation equation is given by

$$\frac{\partial(\rho u_i)}{\partial t}+\frac{\partial(\rho u_i u_j)}{\partial x_j}=-\frac{\partial p}{\partial x_i}+\frac{\partial}{\partial x_j}\left[\mu_{eff}\left(\frac{\partial u_i}{\partial x_j}++\frac{\partial u_j}{\partial x_i}\right)\right]+\rho g_i \tag{2}$$

Here, u_i, u_j represent the velocity components in each respective direction, while x_i and $x_j$denote the coordinate components. The variable ρ refers to the fluid density, p represents the pressure, μ_{eff} denotes the effective viscosity, and g_i stands for the gravitational acceleration in the i-th direction.

In the k-ε model, the mass conservation equations for the water and gas phases are solved independently for each computational grid cell, while a single momentum equation is applied to both phases. The average density is calculated as follows:

$$\overline{\rho}=\alpha_1\rho_1+\alpha_2\rho_2 \tag{3}$$

Here, $\overline{\rho}$ denotes the average density, α_1 and α_2 represent the volume fractions of the first and second phases, respectively, and ρ_1 and ρ_2 refer to the densities of the first and second phases, respectively.

For two-phase flow, the sum of the volume fractions satisfies the following equation:

$$\alpha_1+\alpha_2=1 \tag{4}$$

This approach accounts for the interactions between the phases and is used to determine the average density.

3.3 Turbulence Model

The multiphase flow study of this intake system will utilize the Realizable k-ε turbulence model. In this model, the instantaneous turbulence equations for k and ε are expressed as follows (where $\sigma_k=1.1$, $\sigma_\varepsilon=1.2$, and $C_2=1.9$ respectively):

$$\begin{cases}\frac{\partial(\rho k)}{\partial t}+\frac{\partial(\rho u_i k)}{\partial x_i}=\frac{\partial}{\partial x_i}\left[\left(\mu+\frac{\mu_t}{\sigma_k}\right)\frac{\partial k}{\partial x_i}\right]+\\ +G_k-\rho\varepsilon,\\ \frac{\partial(\rho\varepsilon)}{\partial t}+\frac{\partial(\rho u_i\varepsilon)}{\partial x_i}=\frac{\partial}{\partial x_j}\left[\left(\mu+\frac{\mu_t}{\sigma_\varepsilon}\right)\frac{\partial\varepsilon}{\partial x_j}\right]+\\ +\rho C_1 E\varepsilon-\rho C_2\frac{\varepsilon^2}{k+\sqrt{\upsilon\varepsilon}}.\end{cases} \tag{5}$$

$$C_1=max\left(0.43=\frac{\eta}{\eta+5}\right),$$

$$\eta=\left(2E_{ij}\cdot E_{ij}=\right)^{\frac{1}{2}}\frac{k}{\varepsilon},$$

$$E_{ij}=\frac{1}{2}\left(\frac{\partial u_i}{\partial x_j}+\frac{\partial u_j}{\partial x_i}\right) \tag{6}$$

which is created from turbulent kinetic energy:

$$P_k=\frac{\mu_t}{\rho}\left(\frac{\partial u_i}{\partial x_j}+\frac{\partial u_j}{\partial x_i}\right)\frac{\partial u_j}{\partial x_i} \tag{7}$$

where μ_t, the turbulent dynamic viscosity, is calculated by the following equation:

$$\mu_t=\rho C_\mu\left(\frac{k^2}{\varepsilon}\right) \tag{8}$$

where $C_\mu=0.09$. Constants and functions of the k-ε model are detailed in the study by Yang et al. (2021), which explores advancements in predictive combustion kinetic models and emphasizes model analysis and informative experiments.

The selection of several empirical coefficients in the turbulence model directly influences the calculation results. For complex flows with a free surface, the values of these coefficients play a critical role, and their optimal determination requires extensive testing and computations.

3.4 Mesh Preparation and Independence Analysis

Mesh refinement is applied in regions with significant velocity gradients to reduce numerical diffusion and enhance result accuracy. A mesh independence analysis is performed by comparing flow field results across different grid sizes, demonstrating that further refinement beyond a certain threshold has a negligible impact on the results. The k-ε turbulence model is selected for its robustness and efficiency in handling high Reynolds number flows typical of hydraulic systems. This model solves two transport equations: one for turbulent kinetic energy (k) and another for its dissipation rate (ε), ensuring a balance between computational cost and accuracy.

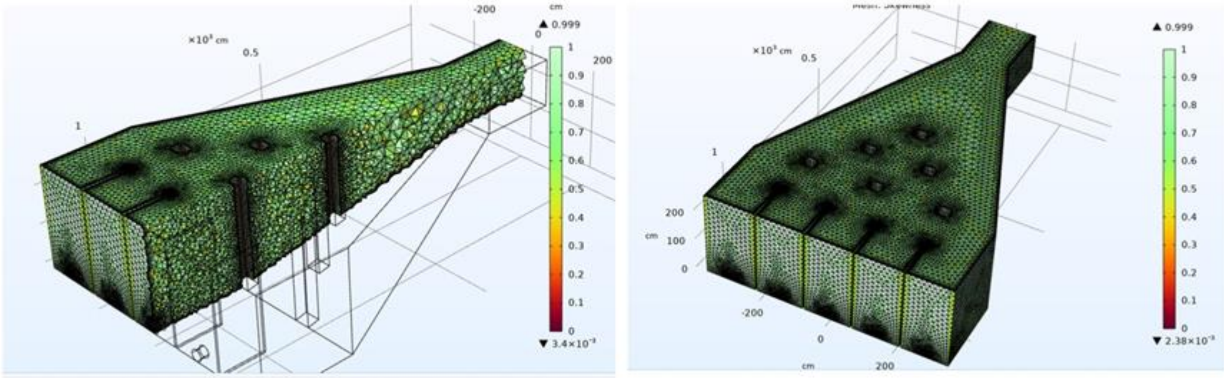

Figure 5*: Grid of the computational domain.*

Slika 5: *Mreža na računskem območju.*

The mesh generation process for each subsystem is illustrated in Figure 5. To ensure computational accuracy, a higher mesh density is generally preferable. However, an excessive number of meshes can lead to high computational costs and reduced efficiency. Therefore, determining the optimal mesh count requires balancing result stability with resource efficiency. For this analysis, seven different mesh resolutions were selected: 0.62 million, 0.75 million, 0.98 million, 1.25 million, 1.6 million, 2.1 million, and 2.6 million. Hydraulic losses, denoted as h_h, were used as the primary criterion for mesh sensitivity analysis.

$$h = \frac{(P_{in} - P_{out})}{(\rho g)} \qquad (9)$$

Here, P_{in} and P_{out} represent the total pressures at the inlet and outlet of the pump station, respectively. The symbol ρ denotes the density of water, taken as 1×10^3 kg/m^3, and g represents the acceleration due to gravity, with a value of 9.81 m/s^2.

Figure 6 illustrates the hydraulic loss trends across different mesh configurations. An inverse relationship is observed between the number of cells and hydraulic losses, where losses decrease as the cell count increases. When the number of cells was below 1.3 million, a significant reduction in hydraulic losses was evident. However, beyond this threshold, further increases in cell count resulted in minimal changes, with variations in hydraulic losses remaining below 2%. This suggests that the selected cell count is sufficient to ensure the required computational accuracy. Consequently, 1.3 million cells were chosen for the remaining simulations.

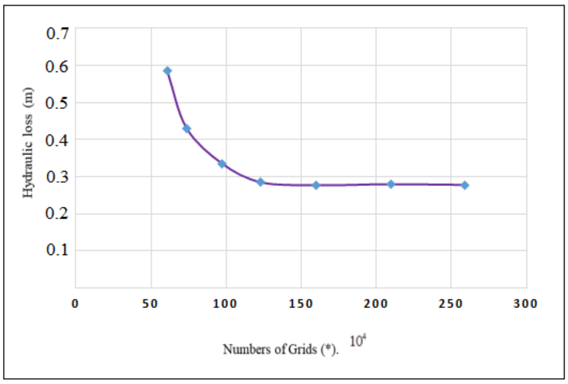

Figure 6: *Hydraulic loss trend chart.*

Slika 6: *Graf hidravličnih izgub.*

3.5. Numerical Scheme

The numerical scheme used for the simulations is based on the finite volume method (FVM), which ensures the conservation of mass, momentum, and energy. The computational domain is discretized using hexahedral control volumes in the bulk regions and tetrahedral elements in complex geometric regions. The mesh independence study confirmed that a grid resolution of 1.3 million cells ensures numerical accuracy while maintaining computational efficiency.

The numerical solution process includes:

- Discretization of the governing equations using FVM.

- Application of the SIMPLE (Semi-Implicit Method for Pressure-Linked Equations) algorithm for pressure-velocity coupling.
- Implementation of the realizable k-ε turbulence model for turbulence closure.
- Definition of boundary conditions at the inlet and outlet regions, with a mass flow inlet and a static pressure outlet.

3.5.1 Mesh Independence Analysis

Mesh refinement was performed in areas exhibiting significant velocity gradients to reduce numerical diffusion and improve result accuracy. The mesh sensitivity analysis indicated that additional refinement beyond 1.3 million cells did not substantially impact the results, with variations in hydraulic losses remaining below 2%.

Boundary Conditions

The boundary conditions for the simulation were established as follows:

Inlet: Fully developed turbulent flow profile with specified velocity magnitude.

Outlet: Static pressure outlet condition.

Walls: No-slip boundary conditions were applied, with wall functions used to account for near-wall turbulence effects.

3.6. Boundary conditions

The flow in the inlet cross-section is already a fully developed turbulent flow, exhibiting significantly greater uniformity. The components of flow velocity in the y and z directions are zero in this cross-section. The velocity in the x direction, referred to as the inlet flow velocity, is established. The unit kinetic energy of turbulence, denoted as k, can be taken as equal to the rate of turbulent dissipation, denoted as ε.

$$K = \frac{3}{2}\left(\frac{U_{ref}}{T}\right)^2 \tag{10}$$

and

$$\varepsilon = C_\mu^{\frac{3}{4}} \frac{k^{\frac{3}{2}}}{L_T} \tag{11}$$

where the special turbulence length (h) is represented by the water depth, U_{ref} represents the velocity of the incoming flow, and T is the initial temperature of the water.

The output flow exhibits characteristics similar to the input flow and has achieved a unidirectional pattern. Excluding its influence on the regional solution calculations downstream of the outlet, the boundary conditions at the outlet are defined as follows: the values of k and ε are maintained at the same levels as those of the input flow.

3.6.1 Boundary conditions free surface

The flow velocity within the inlet channel is low and surface vibrations are minimal. The calculation is based on symmetric boundary conditions, where all variable gradients in the z-direction are set to zero:

$$u \cdot n = 0,$$

$$Kn = -\rho \frac{u_\tau}{u^+} + u\, tan\, g,$$

$$u\, tan\, g = u - (un)n$$

$$\nabla kn = 0,$$

$$\varepsilon = \rho \frac{C_\mu k^2}{K_v \delta_w + \mu} \tag{12}$$

Here, $u^+ = \frac{U}{u\tau}$ is the dimensionless velocity, and $y^+ = \frac{ypu\tau}{v}$ is the dimensionless distance from a node to the wall. Karman constant k is calculated using the relation $k = \frac{u_2}{C_u 0.5}$ and ε represents the roughness constant, which is assumed to be $\varepsilon = 9$ for a smooth wall.

$$\varepsilon = \frac{u_3}{(kY)} \tag{13}$$

Given the significant velocity gradient in the viscous sublayer, the computational grid is refined near the wall. The Reynolds number (Re) is calculated within the resistance region. The computational model employs the RANS approach, with the inlet positioned at the forebay entrance and the outlet located at the water pump's inlet pipe. The influence of flow adjusters installed in the forebay on the flow pattern is analyzed, and the optimal spacing of the columns is determined, as illustrated in Figures 4 and 7.

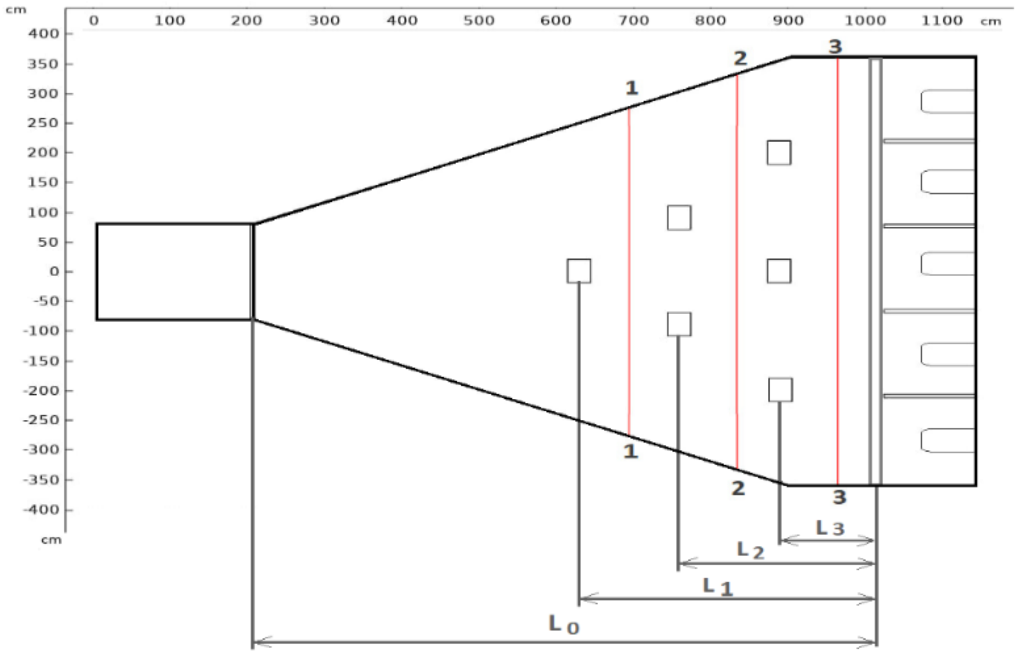

Figure 7*: Schematic diagram of the sections based on which the location of the columns and the flow rate are determined.*

Slika 7: *Shematski prikaz odsekov, na podlagi katerih se določita lokacija stebrov in pretočna hitrost.*

4. Results and discussion

4.1. Flow movement without columns

Due to suboptimal flow distribution in water intake structures, vortices and sedimentation processes can occur. In this study, experiments were conducted with inlet flow velocities of 0.9 m/s and 0.8 m/s (labeled as A1 and A2 in Fig. 8). The primary flow exhibited a high velocity at the cross-section corresponding to the width of the receiving chamber. In regions extending 5 meters on both sides of the forebay, a countercurrent began to develop, leading to the formation of a vortex flow.

4.2. Flow movement in columns

Effective flow velocity distribution in front of an irrigation pumping station is crucial for its operational efficiency. A comprehensive review of the literature on flow regulation in water intake structures and turbulence mitigation guided the strategic arrangement of columns in a checkerboard pattern (see Fig. 7). After the installation of horizontal columns in the pumping station, as illustrated in Figure 8, the formation of large eddies was significantly reduced; however, small eddies were still observed. The presence of columns within the water intake structures decreased the flow rate, improving the alignment of the main flow and effectively minimizing substantial reverse flow on both sides of the forebay chamber. Although small eddies persisted after column installation (see Fig. 9), they did not adversely impact pump operation, and no cavitation phenomena were detected.

4.3. Distribution of flow velocity in the longitudinal section

To correct the flow pattern in a water intake structure (Fig. 7), when the flow enters a column at a specific velocity, it encounters resistance, leading to a small reverse flow on both sides of the column. At the entrance to the water intake chamber, the longitudinal flow velocity is measured at 0.9 m/s at three different depths (Fig. 10). Under free-flow conditions with an unobstructed water surface, velocity gradually increases from the bottom, reaching its peak value at the surface.

An analysis of the surface velocity distribution (Fig. 11) reveals that the maximum velocity around the first pillar is 0.65 m/s, which decreases to 0.55 m/s after the second pillar. Beyond the third-row columns, velocity values range between 0.45 m/s and 0.35 m/s.

When measuring the longitudinal velocity at a depth of h = 1 m from the water level in the forechamber (Fig. 12), it is observed that, at the starting point of the column, the velocity is 0.5 m/s, whereas it decreases to 0.35–0.25 m/s after the third row of columns.

An analysis of the velocity distribution in section 3 (see Fig. 13) reveals that the velocity near the second column reaches a maximum of 0.4 m/s. In conclusion, the results indicate that the flow maintains a consistent velocity throughout the forebay, facilitated by the presence of columns, which effectively minimize the formation of large eddies.

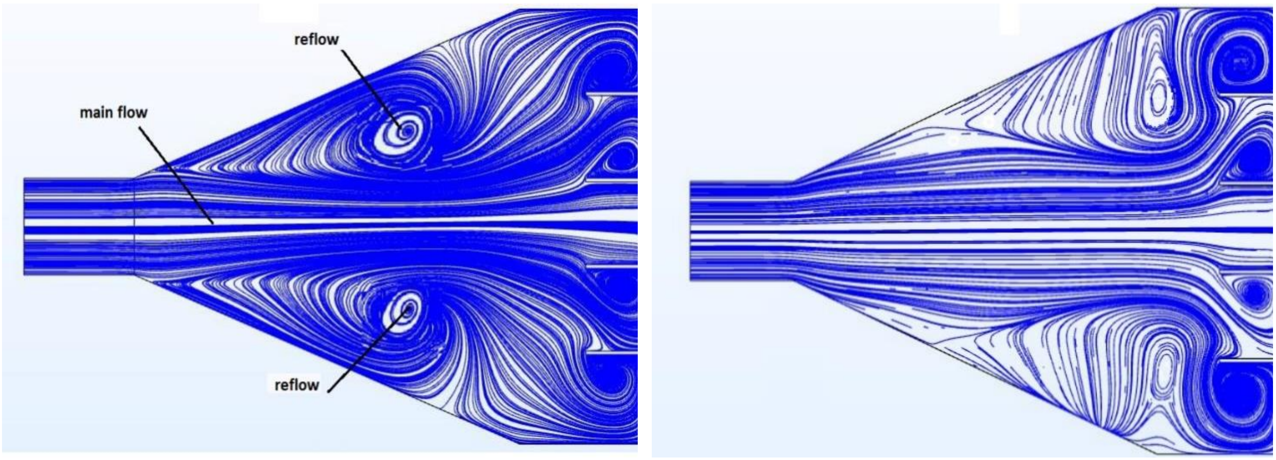

a) A_1 **b) A_2**

Figure 8: *Flow distribution diagram, without rectification in sections A1 and A2.*

Slika 8: *Diagram porazdelitve pretoka brez rektifikacije v odsekih A1 in A2.*

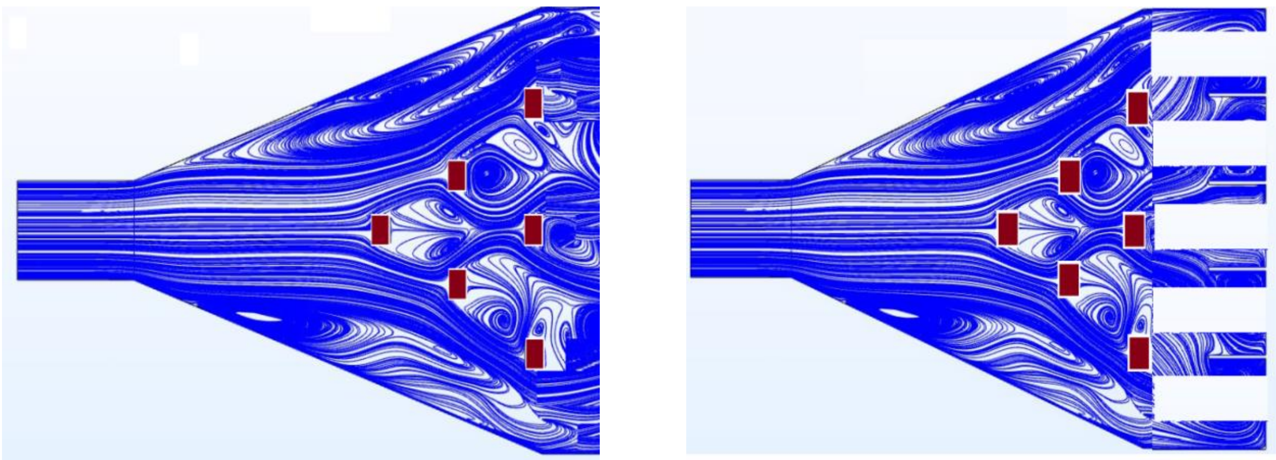

a) A_1 b) A_2

Figure 9: *Flow distribution diagram in sections A1 and A2 of scheme 1–3.*

Slika 9: *Diagram porazdelitve pretoka v odsekih A1 in A2 sheme 1–3.*

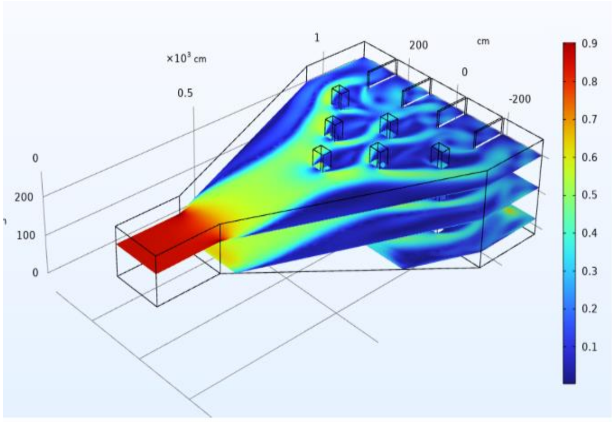

***Figure 10**: Horizontal isolines in 3 different sections.*

***Slika 10**: Horizontalne izolinije v 3 različnih odsekih.*

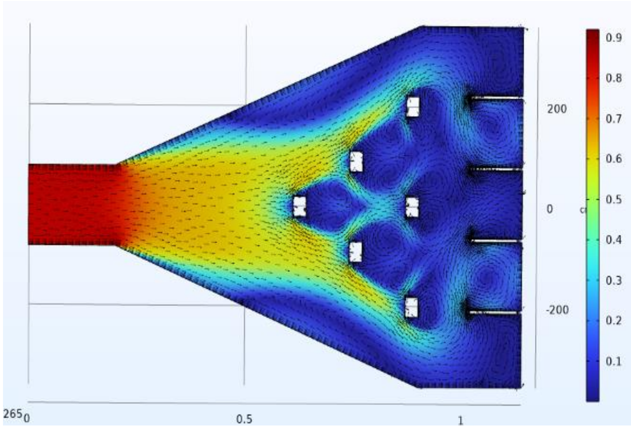

***Figure 11**: Velocity distribution on the water surface.*

***Slika 11:** Porazdelitev hitrosti na vodni gladini.*

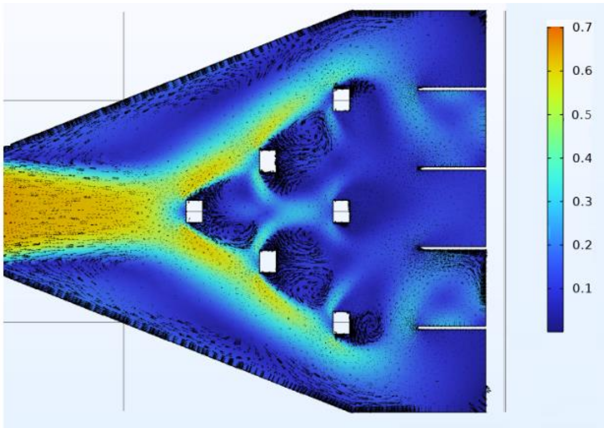

***Figure 12:** Velocity distribution at depth h=1.2 meters.*

***Slika 12:** Porazdelitev hitrosti na globini h = 1,2 metra.*

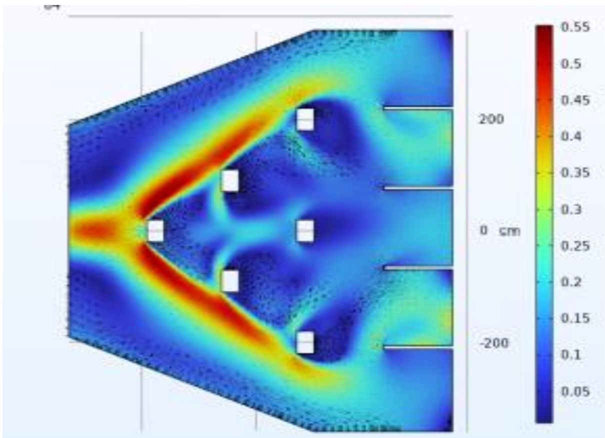

***Figure 13:** Velocity distribution at depth h=1.8 meters.*

***Slika 13:** Porazdelitev hitrosti na globini h = 1,8 metra.*

4.4 Verification of vertical velocity distribution without columns

In the absence of columns installed in the forebay, which divides it into three sections (Fig. 14), the distance of sections 1-1 is measured as L1 = 7 meters from the entrance. At a depth of h = 1.2 meters, the width of this section is b1 = 5.7 meters. Analyzing the speed distribution (Fig. 15) shows that the maximum flow speed at the center reaches 0.61 m/s, while the speed measured 1.1 meters from the wall decreases to 0.03 m/s. This speed reduction can primarily be attributed to the effects of reverse flow. Section 2-2 (Fig. 16) is situated at a distance of L2 = 8.5 meters from the entrance, with a width of b2 = 6.9 meters. The maximum flow speed at this location is 0.53 m/s. Near the shore, the speed increases to 0.05 m/s. At this velocity, sedimentation in the cloud fore-chamber occurs rapidly. In section 3-3 (Fig. 17), the flow behavior exhibits some variation; notably, the highest speed recorded at the center is 0.44 m/s and a sharp increase in speed occurs from 0.13 m/s at a distance of 1.7 meters from the wall.

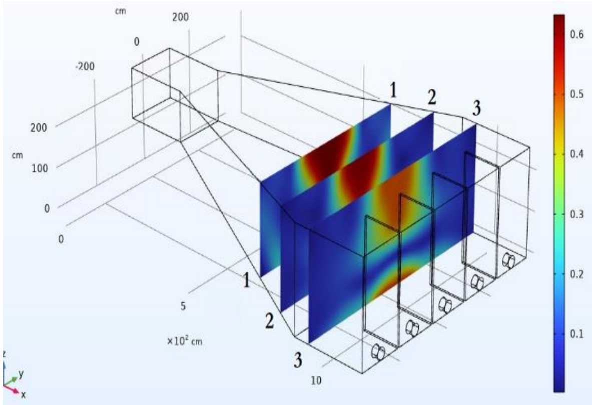

Figure 14: *Flow at a depth of h=1.2 m in the marked areas.*

Slika 14: *Pretok na globini h = 1,2 m na označenih območjih.*

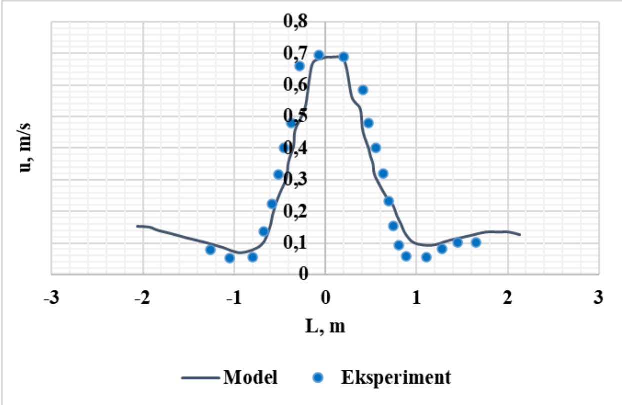

Figure 15: *Flow velocity distribution in section I-I: model and experimental results.*

Slika 15: *Porazdelitev pretočnih hitrosti v odseku I-I: model in eksperimentalni rezultati.*

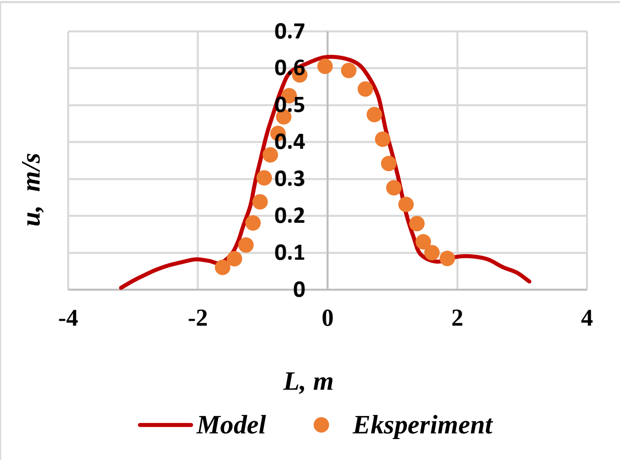

Figure 16: *Flow velocity distribution in section II-II: model and experimental results.*

Slika 16: *Porazdelitev pretočnih hitrosti v odseku II-II: model in eksperimentalni rezultati.*

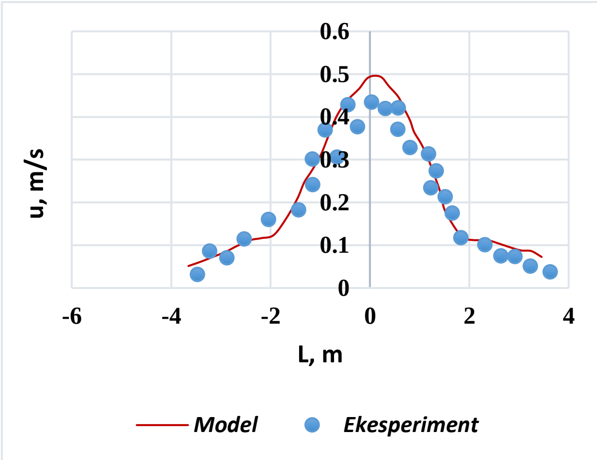

Figure 17: *Flow velocity distribution in section III-III: model and experimental results.*

Slika 17: *Porazdelitev pretočnih hitrosti v odseku III-III: model in eksperimentalni rezultati.*

4.5 Checking the vertical velocity distribution of columns

This section examines the velocity distribution following the vertical installation of columns within the forebay of the pumping station. For this analysis, three gates were positioned perpendicular to the flow direction in the forebay. These gates were strategically placed in the middle of the columns, arranged in a checkerboard pattern, as illustrated in Figures 3 and 18. Considering the velocity distribution at alignment 1-1, which is situated in the forebay, the maximum flow velocity observed at the center was 0.54 m/s in Fig. 19. However, in section 2-2, the velocity decreased to 0.23 m/s at a distance of 2.16 meters from the center (see Fig. 20). Furthermore, at the designated maximum point of section 3-3, the flow velocity reached 0.42 m/s, with an increase to 0.01 m/s noted at a distance of 0.6 meters from the center of the flow (see Fig. 21).

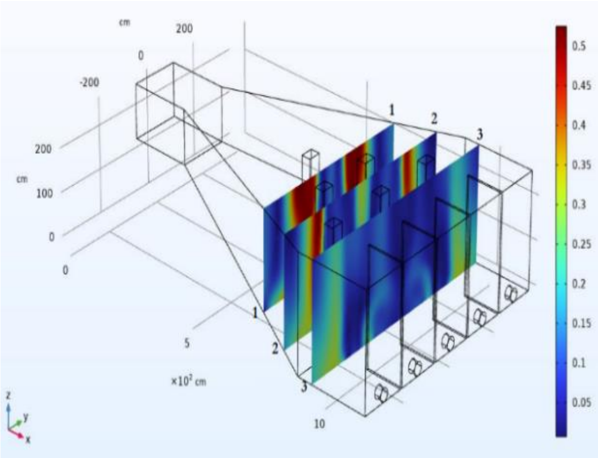

Figure 18: *Flow at a depth of h=1.2 m in the marked areas.*

Slika 18: *Pretok na globini h = 1,2 m na označenih območjih.*

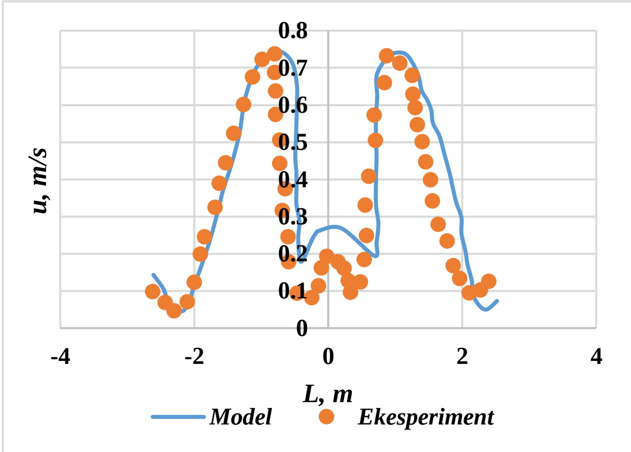

Figure 19: *Distribution of flow velocity in section I-I.*

Slika 19: *Porazdelitev pretočnih hitrosti na odseku I-I.*

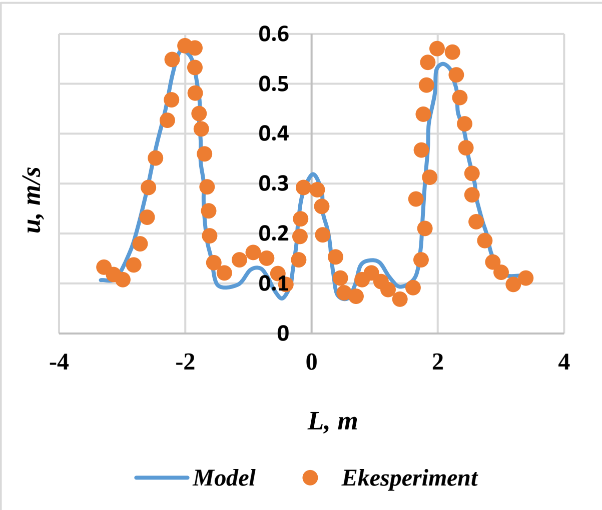

Figure 20: *Flow velocity distribution in section II-II.*

Slika 20: *Porazdelitev pretočnih hitrosti na odseku II-II.*

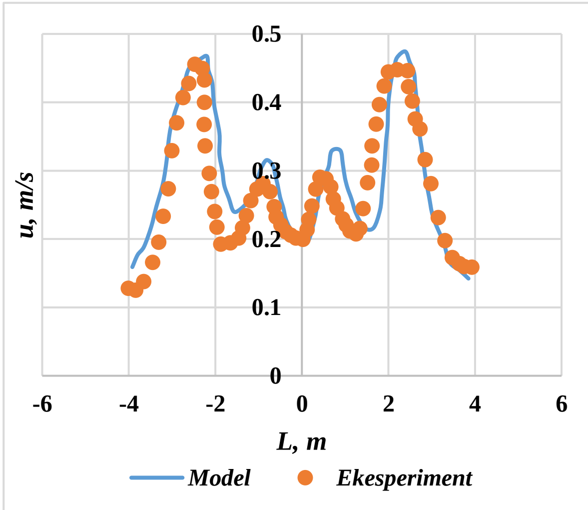

Figure 21: *Flow velocity distribution in section III-III.*

Slika 21: *Porazdelitev pretočnih hitrosti na odseku III-III.*

5. Conclusions

This study presents a comprehensive analysis of flow dynamics within the forebay of a pumping station, employing the k-ε turbulence model in conjunction with advanced numerical simulation techniques. The findings reveal significant flow instabilities in the region near the suction pipe, with velocity fluctuations reaching up to 20% of the intended operational targets. Such discrepancies in flow uniformity pose a substantial risk to the efficiency and safety of the pumping system.

The investigation into the placement of vertical columns highlighted their effectiveness in improving flow uniformity and reducing vortex formation. The strategic arrangement of eight columns in a chessboard pattern enhanced velocity distribution by approximately 15%, significantly mitigating vortex occurrence. However, the limited comparative analysis of different flow rectification strategies necessitates further detailed studies.

To facilitate simulation calculations, a methodological framework was established. Initially, the flow pattern in the forebay was assessed without corrective measures, revealing predominant vortex movement near the lateral walls. Subsequently, various rectification strategies were evaluated to optimize the flow regime and minimize sediment accumulation.

The design specifications for the forebay lengths are as follows: L_0 = 8.2 m, L_1 = 3.6 m, L_2 = 2.4 m, and L_3 = 1.2 m. The strategic installation of flow adjusters at these designated distances produced optimal improvements in flow conditions. It is recommended to install vertical columns with 1-meter spacing to optimize hydraulic performance, as this configuration enhances interaction with the primary flow and minimizes adverse turbulence effects. Furthermore, arranging the columns in a triangular pattern relative to the flow inlet is suggested to maximize flow stability and improve overall hydraulic conditions.

In conclusion, this study provides a solid foundation for future studies by emphasizing the need for a systematic investigation of various flow rectification techniques. Rigorous experimental validation and comprehensive comparative analyses are essential for identifying best practices in hydraulic engineering. These efforts will contribute to the advancement of efficient coastal pumping station designs while ensuring that velocity variations remain below 5%, thereby enhancing operational reliability.

Nomenclature

ρ – density
p – pressure
u_i, u_j – velocity components in each direction
x_i, x_j – represents coordinate components
μ_{eff} – efficiency viscosity
g_i – gravitational acceleration
$\bar{\rho}$ – the average density
α_1 and α_2 – the volume fractions of the first and second phases, respectively
ρ_1 and ρ_2 – the densities of the first and second phases, respectively
P_{in} and P_{out} – the total pressures at the inlet and outlet of the pump station
h – represented by water depth
U_{ref} – the velocity of the incoming flow
T – the initial temperature of the water
FEM – finite element method
k – Karman's constant,
E – the roughness constant,
ν – molecular viscosity
C_1 – first constant in the coefficient of friction
C_2 – second constant in the coefficient of friction
Re – Reynolds number
RANS – Reynolds-Averaged Navier–Stokes

Acknowledgments

The authors would like to express their gratitude to the staff of the Hydraulics Laboratory at Fergana State Technical University for their support in conducting field measurements and experimental modelling. Special thanks are also extended to colleagues who provided assistance with language editing and manuscript proofreading.

CRediT authorship contribution statement

Aybek Arifjanov: Conceptualization, Methodology, Formal analysis, Investigation, Writing – original draft, Supervision. Alimardon Sattorov: Investigation, Resources, Validation, Data curation. Murodil Madaliyev: Software, Data curation, Visualization, Validation, Writing – review & editing. Zokhidjon Abdulkhaev: Project administration, Writing – review & editing, Corresponding author. Mamadali Madrakhimov: Experimental design, Data curation, Visualization.

Data availability

All scientific research data and numerical results used in this study are preserved by the authors and are available upon reasonable request. The modelling results obtained using COMSOL Multiphysics, measurement protocols, and initial experimental datasets are stored at the Hydraulics Laboratory of Fergana State Technical University. For additional information or to request modelling files, please contact the corresponding author.

Declaration of interest

The authors declare that they have no known financial or personal conflicts of interest that could have appeared to influence the work reported in this paper. No generative AI tools were used in the writing or preparation of this manuscript.

Funding

This research did not receive any specific grant from funding agencies in the public, commercial, or not-for-profit sectors.

References

Arifjanov, A., Atakulov, D., Sattorov, A., Melikuziyev, S., Juraboyev, I. (2024). Analysis of the turbidity process in the pumping station forebay for the water management, in: IOP Conference Series: Earth and Environmental Science. IOP Publishing, 12038.

Arifjanov, A. M., Sattorov, A. X., Atakulov, D., Iminov, I. X. (2023). Method of calculation of the flow motion model in water intake facilities, in: IOP Conference Series: Earth and Environmental Science. IOP Publishing, 12060.

Luo, C., Zhang, L., Wang, T., Liu, H., Cheng, L., Lu, M., Jiao, W. (2024). Vortex energy behaviors in the forebay of lateral pumping station for Y-type channel. *Phys. Fluids* **36**(**7**). https://doi.org/10.1063/5.0217558

Mi, Z. H., Zhou, D. Q., Mao, Y. T. (2012). Three-dimensional CFD simulation of solid-liquid two-phase flow in the pumping station forebay with sills, in: IOP Conference Series: Earth and Environmental Science. IOP Publishing, 62027.

Nasr, A., Yang, F., Zhang, Y., Wang, T., Hassan, M. (2021). Analysis of the flow pattern and flow rectification measures of the side-intake forebay in a multi-unit pumping station. *Water (Switzerland)* **13**(**15**). https://doi.org/10.3390/w13152025.

Qiao, Q., Wang, H., Huang, L., Jing, H., Wang, B. (2024). Impact of inlet flow velocity on sediment reduction in pump station forebays. *Phys. Fluids* **36**(**11**). https://doi.org/10.1063/5.0238249.

Shi, W., Lv, F., Yu, X., Wang, X., Ni, C., Lu, W., Xu, L. (2024). Influence of Partition Wall Length on Inlet Flow Regime of a Pumping Station Arranged in Parallel with a Sluice Gate. *Processes* **12**(**4**), 699. https://doi.org/10.3390/pr12040699.

Song, W., Pang, Y., Shi, X., Xu, Q. (2018). Study on the Rectification of Forebay in Pumping Station. *Math. Probl. Eng.* **2018**. https://doi.org/10.1155/2018/2876980.

Xu, C., Zhang, H., Zhang, X., Han, L., Wang, R., Wen, Q., Ding, L. (2015). Numerical Simulation Of The Impact Of Unit Commitment Optimization And Divergence Angle On The Flow Pattern Of Forebay. *Int. J. HEAT Technol.* **33**(**2**), 91–96. https://doi.org/10.18280/ijht.330215.

Yang, F., Zhang, Y., Liu, C., Wang, T., Jiang, D., Jin, Y. (2021). Numerical and experimental investigations of flow pattern and anti-vortex measures of forebay in a multi-unit pumping station. *Water (Switzerland)* **13**(**7**). https://doi.org/10.3390/w13070935,

Ying, J., Yu, X., He, W., Zhang, J. (2020). Volume of fluid model-based flow pattern in forebay of pump station and combined rectification scheme. *J. Irrig. Drain. Eng* **38**, 476–480. https://doi.org/10.3969/j.issn.1674-8530.19.0176.

Zhang, C., Yan, H., Jamil, M. T., Yu, Y. (2022). Improvement of the Flow Pattern of a Forebay with a Side-Intake Pumping Station by Diversion Piers Based on Orthogonal Test Method. *Water* **14**(**17**). https://doi.org/10.3390/w14172663.

Zheng, X., Zhang, P., Zhang, W., Yu, Y., Zhao, Y. (2023). Numerical Study on the Influence of Combined Rectification Facilities on the Flow in the Forebay of Pumping Station. *Water (Switzerland)* **15**(**21**). https://doi.org/10.3390/w15213847.